JCI insight

Pharmacological induction of MHC-I expression in tumor cells revitalizes T cell anti-tumor immunity

Qian Yu, … , Yongjun Dang, Wei Jiang

JCI Insight. 2024. https://doi.org/10.1172/jci.insight.177788.

Research In-Press Preview Oncology

Graphical abstract

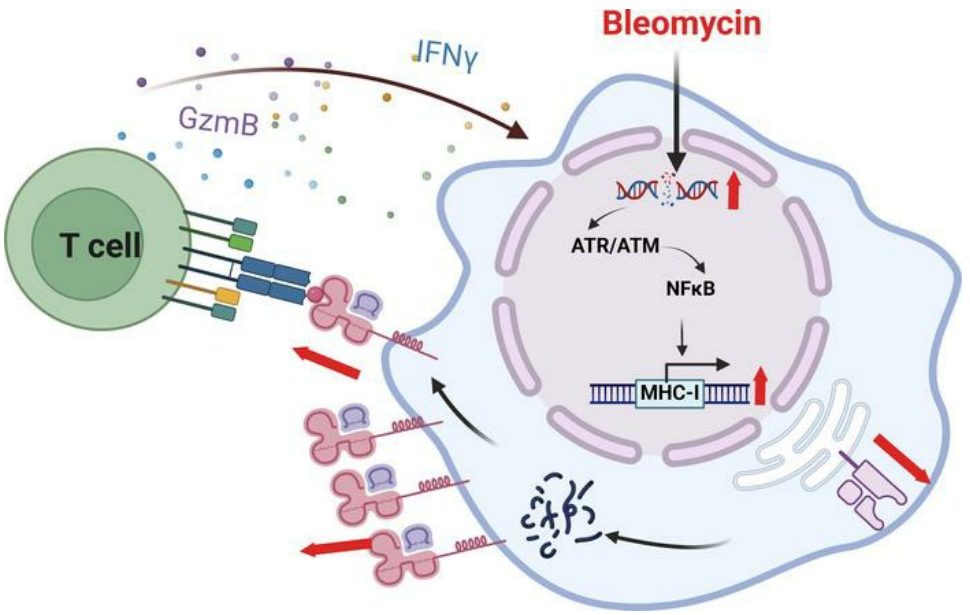

Title: Pharmacological induction of MHC-I expression in tumor cells revitalizes T cell anti-tumor immunity

Authors: Qian Yu[1], Yu Dong[2], Xiaobo Wang[1], Chenxuan Su[2], Runkai Zhang[2], Wei Xu[3], Shuai Jiang[2*], Yongjun Dang[4*], Wei Jiang[1*]

Author Affiliations:

[1]Key Laboratory of Metabolism and Molecular Medicine, Ministry of Education, Department of Biochemistry and Molecular Biology, School of Basic Medical Sciences, Fudan University, Shanghai 200032, China

[2]Department of Urology, Zhongshan Hospital, Fudan University, Shanghai 200032, China

[3]Institute of Immunological Innovation and Translation, Chongqing Medical University, Chongqing; 400016, China

[4]Basic Medicine Research and Innovation Center for Novel Target and Therapeutic Intervention, Ministry of Education, College of Pharmacy, Chongqing Medical University, Chongqing; 400016, China

Address correspondence to: Wei Jiang, Department of Biochemistry and Molecular Biology, School of Basic Medical Sciences, Fudan University, 131 Dong An Road, Shanghai, 200032, China. Phone: 86-18616691036. Email: jiangw@fudan.edu.cn; or Yongjun Dang, Basic Medicine Research and

Innovation Center for Novel Target and Therapeutic Intervention, Ministry of Education, College of Pharmacy, Chongqing Medical University, Chongqing; 400016, China. Phone: 86-13120661770. Email: yjdang@cqmu.edu.cn or yongjundang@fudan.edu.cn; or Shuai Jiang, Department of Urology, Zhongshan Hospital, Fudan University, Shanghai, 200032, China. Phone: 86-13916929866. Email: jiang.shuai@zs-hospital.sh.cn.

Authorship note: Qian Yu and Yu Dong contributed equally to this work.

Conflict of Interests: The authors have declared that no conflict of interest exists.

Abstract

Antigen presentation by Major Histocompatibility Complex Class I (MHC-I) is crucial for T-cell-mediated killing, and aberrant surface MHC-I expression is tightly associated with immune evasion. To address MHC-I downregulation, we conducted a high-throughput flow cytometry screen, identifying bleomycin (BLM) as a potent inducer of cell surface MHC-I expression. BLM-induced MHC-I augmentation renders tumor cells more susceptible to T cells in co-culture assays and enhances anti-tumor responses in an adoptive cellular transfer mouse model. Mechanistically, BLM remodels the tumor immune microenvironment, inducing MHC-I expression in an ATM/ATR-NF-κB-dependent manner. Furthermore, BLM improves T-cell-dependent immunotherapeutic approaches, including bispecific antibodies therapy, immune checkpoint therapy (ICT), and autologous tumor-infiltrating lymphocytes (TILs) therapy. Importantly, low-dose BLM treatment in mouse models amplified the anti-tumor effect of immunotherapy without detectable pulmonary toxicity. In summary, our findings repurpose BLM as a potential inducer of MHC-I, enhancing its expression to improve the efficacy of T-cell-based immunotherapy.

Introduction

Immunotherapy has revolutionized cancer treatment, demonstrating remarkable clinical efficacy across diverse tumor types (1). Despite these achievements, challenges persist, including variable response rates and the evasion of immune surveillance by malignant cells representing marked hurdles (2, 3). A pivotal mechanism in immune evasion is the downregulation of cell surface Major Histocompatibility Complex Class I (MHC-I), compromising T-cell-mediated killing (2, 4, 5).

Human MHC-I molecules, commonly known as HLA, play a crucial role in antigen presentation to T cells and tumor immune escape (6). Previous studies underscore a positive correlation between MHC-I expression and patient prognosis across various cancer types (7). Conversely, downregulation of MHC-I has been associated with disease progression and unfavorable prognosis in diverse cancers, such as breast carcinoma (8), colon carcinoma (9), Hodgkin Lymphoma (10), non-small cell lung cancer (11), and bladder carcinomas (12). Importantly, reduced MHC-I expression has been linked to resistance to immune checkpoint therapy (ICT) (13), where the therapeutic efficacy relies on cytotoxic T cells recognizing cytosolic antigens presented by MHC-I on the tumor cell surface (14, 15).

Diverse strategies employed by malignant cells to subvert immune surveillance underscore the crucial need for identifying effective small molecules capable of overcoming these evasion mechanisms. While immune

checkpoint blockage has proven to be a pivotal therapeutic strategy to thwart immunosurveillance, the focus has predominantly centered on antibodies. Small molecules targeting PD-1/PD-L1 function have also emerged and entered to clinical trials. However, investigations into molecules specifically regulating MHC-I expression have been comparatively limited. Notably, previous observations have demonstrated increased MHC-I expression following treatment with cyclin-dependent kinase 4 and 6 (CDK4/6) inhibitors or the EZH2 inhibitor GSK126 for seven days (16, 17), indicating the potential of small molecules in regulating MHC-I expression. However, there is a need to explore effective strategies for improving MHC-I expression and function.

The expression of MHC-I is regulated by multiple regulators and pathways including IRF1, STAT1 and NRF5 (18). Among them, the transcription factor NF-κB plays a crucial role in the regulation of MHC-I (19). Activation of NF-κB was shown to promote increased expression of MHC-I and counter the immune evasion employed by cancer cells (20, 21).

In this context, the present study aims to address the challenge of low MHC-I expression on tumor cells. Leveraging a high-throughput flow cytometry system, we systematically screened for small molecules capable of rapidly enhancing surface MHC-I expression. Our investigations led to the identification and validation of bleomycin (BLM) as a potent inducer of MHC-I expression in tumor cells. Renowned as an antibiotic chemotherapeutic agent with established applications in various cancers, the clinical use of BLM has

been constrained by its side effect on lung injury. This investigation delves into the multifaceted effects of BLM. Our study unveils BLM's ability to promote $CD8^+$ T cell activation through antigen-dependent mechanisms, a phenomenon that is substantiated both ex vivo and in vivo. Moreover, BLM emerges as a regulator of the tumor immune microenvironment, inducing MHC-I expression in a manner dependent on ATM/ATR-NF-κB signaling. Importantly, our findings indicate the synergistic potential of low-dose BLM treatment when combined with immunotherapy and DNA methyltransferase inhibitors, all while avoiding detected toxicity. To validate the translational impact of our study, we extended our findings to a clinically relevant experimental setting. Here, BLM demonstrates its ability to heighten the susceptibility of patient-derived tumor cells to cytotoxicity mediated by autologous tumor-infiltrating lymphocyte (TILs). This not only underscores the potential clinical relevance of BLM but also repurposes it as a key player in enhancing the efficacy of immunotherapeutic interventions.

Results

BLM upregulates MHC-I expression

To identify drugs with the potential to notably upregulate MHC-I expression, we conducted a screening of 2,112 FDA-approved drugs utilizing a high-throughput flow cytometry system based on tumor cell surface MHC-I expression. This screening identified several compounds, including BLM sulfate, etoposide, cabazitaxel, entinostat, and CI994, as robust enhancers of MHC-I expression (Supplemental Figure 1). Notably, the ability of paclitaxel to promote MHC-I expression in tumor cells has been previously reported (7), explaining the similar capability observed in cabazitaxel, an analog of paclitaxel. Etoposide (7) and HDAC inhibitors such as entinostat and CI994 have also demonstrated their ability to modulate MHC-I expression in cancer cells (22-24). Therefore, we focused our further investigations on BLM, an antibiotic chemotherapeutic drug.

Flow cytometry analysis unequivocally demonstrated a dose- and time-dependent increase in MHC-I cell surface expression in SU-DHL-4 cells following BLM treatment (Figure 1, A-D). In addition, HLA-A protein levels showed a parallel increase in a time- and dose-dependent manner in both SU-DHL-4 (Figure 1, E and F) and SK-BR-3 (Supplemental Figure 2A) cells. Specifically, genes encoding MHC-I molecules (*HLA-A*, *HLA-B*, *HLA-C*, and *B2M*), peptide transport (*TAP1* and *TAP2*), transporter-MHC interactions (*TAPBP*), and peptide degradation (*PSMB8* and *PSMB9*) were upregulated in

BLM-treated SU-DHL-4 (Figure 1G) and SK-BR-3 (Supplemental Figure 2A) cells. Moreover, in vitro BLM treatment induced increased MHC-I expression in various human tumor cell lines, including T-47D, MDA-MB-231, and BT549 (Supplemental Figure 2, B-D). Also, besides HLA-A, the expression level of HLA-B and HLA-C were also increased following BLM treatment in SK-BR-3 cells, indicating that BLM acted in an allele-independent manner (Supplemental Figure 2E). Importantly, BLM exhibited a lasting effect on the induction of MHC-I expression, persisting even after drug retrieval (Supplemental Figure 2F). Analysis of The Cancer Genome Atlas (TCGA) data confirmed that the BLM-treated signature correlated with MHC-I expression in human cancers, showing a positive correlation across numerous cancer types with gene signatures of the MHC Class I pathway (Supplemental Figure 2F). Notably, in certain cancer types, such as LUSC and SARC, the BLM-treated signatures exhibited a negative correlation with the pathway. (Supplemental Figure 2F), which was possibly due to the heterogeneity between different tumor types.

The BLM-induced increase in cell surface MHC-I expression was also evident in murine tumor cell lines (B16F10, MC38, and MB49) (Supplemental Figure 3, A-C). Western blot analysis further confirmed a dose- and time-dependent increase in murine B2M protein levels on B16F10 cells following BLM treatment (Supplemental Figure 3D). Similarly, genes encoding murine MHC-I molecules (*H2d1*, *H2k1*, and *B2m*), those governing peptide transport

(*Tap1* and *Tap2*), and those involved in peptide degradation (*Psmb9*) were upregulated in BLM-treated murine cells (Supplemental Figure 3E). Collectively, these findings underscore the effective role of BLM in enhancing MHC-I expression in tumor cells.

BLM-mediated increase in peptide-MHC-I complexes primes $CD8^+$ T cell activation by antigen-dependent mechanism

Given the observed upregulation of antigen presentation gene expression by BLM, we hypothesized that it might enhance the function of MHC-I in antigen presentation. To investigate this hypothesis, we employed a peptide pulsing assay to evaluate cell surface expression of peptide-MHC-I complexes. Following peptide pulsing, B16F10 cells exhibited inadequate presentation of MHC-I-bound SIINFEKL complexes, an 8-amino acid peptide derived from OVA. However, pre-treatment with BLM dramatically enhanced the expression of these complexes (Supplemental Figure 4, A-D). Similarly, the murine cell line B16OVA, expressing ovalbumin (OVA), exhibited an increase in MHC-I-bound SIINFEKL complexes upon BLM treatment, indicating that BLM enhances antigen presentation. (Supplemental Figure 4, E and F).

Solid tumors often evade anti-tumor immunity by downregulating MHC-I surface expression, resulting in reduced recognition and responses by $CD8^+$ T cells (7). To investigate whether the increase in peptide-MHC-I complexes

induced by BLM enhanced $CD8^+$ T cell activation and tumor-killing capability, we conducted a co-culture assay of B16OVA tumor cells and OT-I T cells. Importantly, BLM pre-treated B16OVA tumor cells exhibited increased susceptibility to the cytotoxicity of MHC-I-restricted OVA-specific $CD8^+$ T cells (pre-activated OT-I T cells) compared to the control group. This was evidenced by a lower number of viable tumor cells, a higher apoptosis rate, and increased Interferon-gamma (IFN-γ) production (Figure 1, H-J). In contrast, B16F10 cells, owing to the absence of the cognate antigen OVA, remained resistant to OT-I T cell killing and failed to induce T cell cytokine production, even when exposed to relatively low concentrations of BLM (Figure 1, H-J). In line with this, TCGA analysis revealed a positive correlation between the BLM-treated signature and $CD8^+$ T cell activation in several human cancers (Supplemental Figure 4G). These results clearly demonstrate that BLM treatment sensitizes tumor cells to $CD8^+$ T cell-mediated killing.

Additionally, we utilized human $CD8^+$ T cells that were engineered with a recombinant T cell receptor (TCR) targeting the NY-ESO-1 antigen (specifically the NY-ESO-1:157–165 epitope) in an HLA-A*02-restricted fashion (referred to as ESO T cells) (25). Then we performed the co-culture assay of NY-ESO-1^+ SK-BR-3 cells and ESO T cells to examine the effect of BLM in the scenorio of human cancer (Supplemental Figure 5, A and B). Consistent with the results from the co-culture assay of B16OVA cells and OT-I T cells, NY-ESO-1^+ SK-BR-3 cells pre-treated with BLM showed

significantly increased apoptosis rates compared to the control group (Supplemental Figure 5, C and D). This indicates that BLM treatment sensitizes human cancer cells to $CD8^+$ T cell-mediated killing.

To examine whether BLM treatment affects antigen-independent activation of T cells, an ex vivo splenocyte culture assay was employed (26). Splenocytes treated with BLM or Concanavalin A (Con A, an antigen-independent mitogen) for 24 h were analyzed using flow cytometry to assess the frequency of $CD44^+$ and $CD69^+$ markers, which are indicative of T cell activation among $CD8^+$ or $CD4^+$ T cells (Supplemental Figure 6A). As expected, Con A induced the expression of $CD44^+$ and $CD69^+$ markers in $CD8^+$ cells or $CD4^+$ T cells, while BLM treatment had no such effect (Supplemental Figure 6, B-E). This firmly rules out the possibility of antigen-independent activation of T cells following BLM treatment.

In summary, these results confirm that BLM treatment promotes $CD8^+$ T cell activation through antigen-dependent mechanisms.

BLM potentiates the anti-tumor responses of T cells in vivo

To investigate the anti-tumor effect of BLM in vivo, we used combination of BLM and adoptive T cell transfer. To determine an effective anti-tumor concentration, we noticed in a previous study that a low dose (5 mg/kg) of BLM moderately reduced tumor volume without significant changes in mouse weight or evident lung toxicity (27). Therefore, we selected 3 mg/kg BLM for

subsequent experiments.

We investigated whether the combination of BLM and the infusion of OT-I cytotoxic T lymphocytes could enhance the killing efficacy of OT-I cells in an adoptive cellular transfer mouse model (Figure 2A). All treated groups exhibited body weights similar to those of the vehicle group (Figure 2B). To assess potential lung toxicity, a primary adverse effect of clinical BLM uses in cancer treatment (27), we conducted H&E staining, revealing no discernible lung damage in either the BLM treatment group or the combination treatment group (Supplemental Figure 7).

Mice treated with a relatively lower dose of BLM alone did not exhibit a remarkable anti-tumor response. Infusion of OT-I cells alone led to a slowdown in tumor growth, whereas the combination treatment resulted in further reductions in tumor weight (Figure 2C) and tumor volume (Figure 2D) compared to mono-OT-I cell therapy. Additionally, western blot analysis demonstrated that BLM elevated B2M expression in tumor samples (Figure 2E). Immunofluorescence staining of tumor tissues revealed slightly increased infiltration of granzyme B^+ cells in the BLM-treated group compared to that in the vehicle group. Importantly, the combination treatment group exhibited a higher percentage of granzyme B^+ cells than the mono-OT-I cell therapy group (Figure 2F). Further analysis indicated that combination treatment significantly upregulated the gene expression of granzyme B, IFN-γ, and perforin, secreted by cytotoxic $CD8^+$ T cells (Figure 2G). BLM also sensitized

B16OVA melanomas to OT-I cell transfer therapy, resulting in a substantial survival benefit (Figure 2H).

To assess whether BLM influenced T cell homing to tumors, we employed BrdU analysis to track T cells division in tumors after intravenous transfer of pre-activated CD45.1^{+} OT-I cells into B16-OVA tumor-bearing mice for three days. Notably, the combination treatment group exhibited a higher density of OT-I cells in tumors than the monotherapy group with OT-I cell infusion (Figure 2, I and J). However, there was no difference in the percentage of proliferating of OT-I cells among tumors in tumor-bearing mice following treatment with OT-I cells alone or in combination with BLM and OT-I cells, as measured by BrdU incorporation (Figure 2K), indicating that the increased T cell homing, instead of T cell proliferation, was responsible for the effect of BLM.

In summary, these findings suggest that BLM treatment enhances T cell homing to tumors, thereby amplifying the anti-tumor responses of OT-I cells in adoptive T cell therapy in a mouse model.

MHC-I is indispensable for the effect of BLM on promoting T cell anti-tumor immunity

To ascertain the role of antigen recognition by cancer cells in BLM's anti-tumor effects, we conducted knockdown (KD) experiments targeting *B2m*, a pivotal component of MHC-I molecules, in B16OVA cells (Supplemental

Figure 8A). When co-cultured with OT-I T cells, BLM enhanced the susceptibility of B16OVA cells to $CD8^+$ T cell killing, whereas *B2m* KD B16OVA cells remained resistant to OT-I T cells (Figure 3A). T cell activation, as indicated by IFN-γ release, returned to the control levels when *B2m* was disrupted in B16OVA cells (Figure 3B). Moreover, we observed that the levels of STAT1 phosphorylation and PD-L1 expression after IFN-γ treatment were unaffected by MHC-I inhibition (Supplemental Figure 8, B-D).

Subsequently, we implanted *B2m* KD B16OVA clones into mice and assessed the anti-tumor effect of BLM in combination with OT-I cytotoxic T lymphocyte infusion in adoptive T cell transfer therapy (Figure 3C). While BLM treatment alone led to a modest decrease in tumor growth in the negative control clone, this effect was significantly amplified when combined with OT-I T cells (Figure 3, D and E). In contrast, the disruption of *B2m* in B16OVA cells attenuated the anti-tumor effect mediated by OT-I T cells, rendering the combination treatment with BLM ineffective in slowing tumor growth (Figure 3, D and E).

To further confirm that the increased T cell killing effect of BLM was dependent on the upregulation of MHC-I expression, we overexpressed the *H2k1* gene in B16OVA cells to increase the surface expression of $H\text{-}2K^b$ (Figure 3F). In B16OVA cells overexpressing the *H2k1* gene pretreated with BLM, no significant increase in T cell-mediated cytotoxicity was observed when co-cultured with OT-I T cells compared to the control group (Figure 3, G

and H). This suggests that the effect of BLM is dependent on the upregulation of MHC-I.

In summary, these findings underscore the substantial impact of MHC-I on anti-tumor effect of BLM.

BLM treatment remodels the tumor microenvironment

To investigate the potential molecular mechanism of anti-tumor responses of BLM treatment in B16-F10 melanoma, we performed unsorted Single-cell RNA sequencing, yielding 26,954 high-quality transcriptomes after quality control and filtering (Supplemental Figure 9A). To determine which cellular compartments that account for the highest BLM efficacy, we analyzed single-cell transcriptomes for the expression of melanoma, immune, fibroblast, and stromal marker genes. Consistent with above results, BLM treatment group exhibited an overrepresentation of immune cell transcriptomes compared to the control group (Figure 4A). Next, we subset and re-clustered immune cells into macrophages, monocytes, dendritic cells (DC), T cells, and neutrophils (Supplemental Figure 9B). We employed the Cellchat package to compute the total number of interactions and interaction strength of the inferred cell-cell communication networks, which were both significantly increased after BLM treatment (Figure 4B). We also observed significantly increased cell-cell interaction strength and interaction numbers among different cell types, especially signals sent from melanoma to other cell types, in the BLM group

compared with those in the control groups (Supplemental Figure 9, C and D). To further dissect the influence of BLM within the melanoma cell compartment, melanoma cell transcriptomes were subset and re-clustered into six subclusters named Mel0 to Mel5 by UMAP analysis (Figure 4C). The CNV scores in the BLM group among the six melanoma subclusters (Mel0 to Mel5) were significantly lower than those in the control group (Figure 4D). Using CytoTRACE, we observed that the Mel3 subcluster with the highest CytoTRACE score (Supplemental Figure 9, E and F), which was regarded as the starting point of the trajectory by monocle3. We suggested that the ends of the pseudotime trajectories of the other melanoma subclusters were the different end states of the cancer cells (Supplemental Figure 9G). Additionally, we found that the BLM group was more differentiated, which indicated a less malignant phenotype (28) (Supplemental Figure 9H).

Subsequently, we performed GO enrichment analysis to investigate the various biological processes of melanoma sub-clusters (Supplemental Figure 10, A-C). The Mel1 subcluster enriched DNA proliferative pathways such as “DNA replication,” “nuclear division,” “chromosome segregation,” suggesting that it was at a relatively high proliferative status (Supplemental Figure 10, A-C). The Mel3 subcluster enriched MHC-I related pathways such as “TAP2 binding,” “TAP1 binding,” “TAP binding,” “MHC class I peptide loading complex” (Figure 4E). Therefore, we regarded the Mel3 sub-cluster as the MHC-I-active sub-cluster. Additionally, compared with the control group, the

BLM group showed an increase in Mel3 subcluster transcriptomes and a decrease in Mel1 subcluster transcriptomes (Figure 4C). Subsequently, we used high-dimensional weighted gene co-expression network analysis (hdWGCNA) to determine the main molecular characteristics of Mel3. We identified thirty gene modules, and the functions of the M25 module were associated with the MHC class I protein complex pathway (Figure 4F). Moreover, the hub genes (*H2-D1*, *H2-K1*, *B2m*, *H2-T22*, and *H2-T23*) of M25 were also closely related to the MHC-I pathway (Figure 4G).

We quantified oncogenic signal strengths using pathway target gene signature expression and discovered that the BLM group exhibited elevated activity in many signaling pathways, including JAK-STAT, NF-κB, TNFα, p53, VEGF, EGFR, TGFβ, and WNT, as well as in hypoxia-induced pathways. In contrast, the control group exhibited low activity for these pathways (Supplemental Figure 10D). The activities of TGFβ, VEGF, EGFR, WNT, p53, NF-κB, TNFα signaling, and hypoxia-induced pathways increased to varying degrees after BLM treatment in the Mel3 subcluster, suggesting that these pathways might be involved in the regulation of MHC-I expression (Figure 4H).

Consistent with our previous experimental results, single-cell RNA analysis further verifies that BLM treatment enhances immune cell infiltration, reduces the degree of malignancy and differentiation potential of melanoma cells, and promotes MHC-I-active subcluster expression, which reveals the anti-tumor efficacy of BLM.

MHC-I upregulation caused by BLM depends on ATM/ATR-NF-κB activation

We used LISA (29) to identify key transcription factors that drove changes in gene expression caused by BLM treatment, highlighting specific transcription factors linked to BLM. This analysis predicted that RELA most likely influenced the upregulated differentially expressed genes (Figure 5A). Additionally, MHC-I expression is regulated by various transcription factors that bind to the MHC-I promoter (30). Among these, IRF-1 (31), NF-κB (7), and NLRC5 (32) are crucial for the transcriptional upregulation of MHC-I genes following cytokine stimulation. Intriguingly, NF-κB was significantly induced following BLM treatment (Supplemental Figure 11A). Moreover, the levels of phosphorylated p65 significantly increased after BLM treatment (Figure 5B). To investigate whether NF-κB plays a role in BLM-induced MHC-I upregulation, we pre-treated SK-BR-3 cells with or without the NF-κB inhibitor BAY11-7082. BAY11-7082 reversed the BLM-induced upregulation of HLA-A and phosphorylated p65 caused by BLM treatment (Figure 5C). Notably, HLA-A expression showed no significant change upon BLM treatment in the *P65* knockdown groups (Figure 5D). qRT-PCR analysis confirmed that the increased mRNA expression of *HLA-A*, *HLA-B*, and *HLA-C* after BLM treatment was also blocked by the knockdown of *P65* (Figure 5E). Furthermore, BLM treatment led to dose- and time-dependent reduction in IκB

protein levels (Supplemental Figure 11, B and C). Collectively, these data indicate that NF-κB activation plays a critical role in BLM-induced MHC-I upregulation.

BLM possesses radiomimetic properties, induces DNA double-strand breaks, and is widely used in clinical chemotherapy for various cancers (33). Consistent with previous studies, we observed dose- and time-dependent increases in the expression of DNA damage response markers, including γH2AX (S139), phosphoATM (S1981), and p53 (S15), following BLM treatment (Supplemental Figure 11, D and E). Furthermore, immunofluorescence revealed an elevated number of γH2AX foci in SK-BR-3 cells after BLM treatment (Figure 5F). To assess whether MHC-I upregulation due to BLM was influenced by the DNA damage response pathway, we pre-treated cells with an ATM inhibitor (Ku60019), ATR inhibitor (AZD6738), or DNA-PKcs inhibitor (NU7441) before subjecting them to BLM treatment for 48 h. BLM-induced MHC-I upregulation was diminished in ATM or ATR inhibitor-pre-treated cells (Figure 5G), but not in DNA-PKcs inhibitor-pre-treated cells (Supplemental Figure 11F). In summary, these findings suggest that MHC-I upregulation following BLM treatment is contingent on ATM/ATR-NF-κB activation.

The activated cyclic GMP–AMP synthase (cGAS)/stimulator of interferon genes (STING) pathway also promotes MHC-I mRNA expression by increasing the expression of type I interferon (IFN-α/β) (34, 35). Therefore, we

explored whether the cGAS-STING pathway is activated by BLM treatment. Our results, following *STING* knockdown, indicated that the cytosolic DNA-sensing pathway was not necessary for MHC-I induction after BLM treatment in SK-BR-3 cells (Supplemental Figure 11G). Similarly, MHC-I expression remained unchanged after BLM treatment in the suppression of *TRAF6* (Supplemental Figure 11H). Additionally, the tumor suppressor p53, a crucial effector of the DNA damage response, is phosphorylated and activated by various DNA damage-inducible kinases including ATM(36). Previous studies have shown that p53 expression increases following BLM treatment (37). We speculated that p53 played a role in BLM-induced MHC-I upregulation. However, MHC-I expression showed no significant difference after BLM treatment in *TP53* knockdown cells (Supplemental Figure 11I). Consequently, p53 was deemed unnecessary for MHC-I induction following BLM treatment.

IFN-γ secreted by activated T cells, plays a pivotal role in the activation of cellular immunity and, consequently, the stimulation of anti-tumor immune responses (38). We investigated whether BLM treatment enhances the IFN-γ-induced transcriptional response in tumor cells. Gene Set Enrichment Analysis (GSEA) showed that IFN-α/γ and inflammatory pathways were transcriptionally activated in BLM-treated tumor cells (Figure 5H). Furthermore, we observed that BLM induced additional MHC-I upregulation in the presence of a relatively low dose of IFN-γ, suggesting that BLM enhances HLA presentation through an IFN-independent mechanism (Figure 5I and

Supplemental Figure 11, J and K).

In summary, our data demonstrate that BLM-induced MHC-I upregulation in tumor cells relies on ATM/ATR-NF-κB activation.

DNA methyltransferase inhibition synergizes with BLM to induce anti-tumor immune responses

Cytidine methylation reduces the efficiency and alters the pattern of BLM-mediated cleavage of double-stranded DNA (39). Thus, we posited that DNA methyltransferase inhibitors (DNMTi) would promote the anti-tumor immune effect of BLM. Sequential treatment with DNMTi and BLM demonstrated a synergistic and robust potentiation of BLM by DNMTi in SK-BR-3 cells (Figure 6A and Supplemental Figure 12A). Among the DNMTi tested, decitabine (DAC) in combination with BLM exhibited the most potent antiproliferative effect compared to azacitidine (AZA), and was therefore chosen for further investigation. MHC-I expression was increased with the combined treatment of BLM and DNMTi (Supplemental Figure 12B). Consistent with previous data, both BLM and DAC (39, 40) induced a DNA damage response, as evidenced by γH2AX foci accumulation in SK-BR-3 cells (Supplemental Figure 12, C and D). Furthermore, DNMTi potentiated BLM-mediated DNA damage, as indicated by higher expression of γH2AX S139 and increased γH2AX foci accumulation (Supplemental Figure 12, C and D).

We also observed a potent augmentation of the BLM antiproliferative

effect in B16F10 tumor cells when used in combination with DAC (Supplemental Figure 12E). Additionally, we explored the potential of DAC treatment to enhance BLM-induced T cell activation. Neither BLM nor DAC treatment alone resulted in fewer viable cancer cells than the control group after co-culture with OT-I T cells. However, there was a significant potentiation of the BLM-induced T cell activation when used in combination with DAC (Figure 6, B and C). We further examined the impact of DAC on tumor response to BLM treatment in vivo by treating established B16F10 melanoma tumors with DAC and/or BLM. There were no significant differences in mouse body weight among the different treatment groups (Figure 6D). Consistent with the in vitro co-culture results, DAC treatment alone moderately slowed tumor growth in vivo, and the combination treatment of DAC and BLM further reduced tumor progression (Figure 6, E and F).

In summary, DNMTi enhances the upregulation of MHC-I in tumor cells induced by BLM and facilitates cancer cell killing by T cells, thereby complementing the therapeutic effects of BLM in B16F10 xenografts.

BLM-mediated potentiation of anti-tumor responses for T-cell-based immunotherapy

We further investigated the potential of combination therapies with BLM in immunotherapy approaches, such as bispecific antibody, immune checkpoint therapy and TILs therapy in solid tumors, which efficacy were all relied on T

464 cells and were restricted by MHC-I expression levels.

465 A recent study introduced a bispecific antibody (H2-scDb) designs to
466 specifically target the most common p53 mutation (R175H) along with a
467 common HLA-A allele (HLA-A*02:01) on the cell surface. The efficacy of H2-
468 scDb is highly correlated with the levels of HLA-A allele (HLA-A*02:01)
469 expressed in tumor cells (41). We demonstrated dose- and time-dependent
470 increase in surface HLA-A2 levels in SU-DHL-4 ($p53^{WT}$ and HLA-A*02:01) and
471 SK-BR-3 ($p53^{R175H}$ mutation and HLA-A*02:01) cells after BLM treatment
472 (Supplemental Figure 13, A and B). We then examined whether BLM
473 treatment could enhance the ability of H2-scDb to activate T cells. Consistent
474 with previous studies, H2-scDb had no impact on SK-BR-3 cells, which
475 harbored the $p53^{R175H}$ mutation and exhibited relatively low expression of
476 HLA-A*02:01. However, pre-treatment with BLM enhanced T cell activation
477 mediated by H2-scDb, resulting in a higher number of tumor cells killing and
478 higher production of IFN-γ (Figure 7, A-C).

479 Many solid tumors resistant to checkpoint blockade are characterized by a
480 lack of cytotoxic T cells recognition and infiltration (42). Therefore, we
481 hypothesized that BLM might enhance the efficacy of checkpoint blockade by
482 increasing MHC-I expression and promoting T-cell infiltration. To investigate
483 whether the anti-tumor efficacy of PD-L1 blockade could be improved by
484 combination with BLM treatment, we treated B16F10 melanoma-bearing mice
485 with BLM, anti-mouse PD-L1 antibody, or a combination of both. The body

weight remained stable across the different treatment groups (Figure 7D). Furthermore, mice treated with BLM or PD-L1 antibody alone showed partial tumor growth inhibition, while BLM sensitized B16F10 melanomas to checkpoint blockade with a PD-L1 antibody, resulting in substantially reduced tumor growth and tumor weight (Figure 7, E and F). Additionally, the effect of BLM was examined in MC38 mouse model and similar results were obtained (Supplemental Figure 14, A-D).

We next expanded our results to a clinically relevant experimental setting. Tumors with high levels of somatic mutations, such as melanoma and bladder cancer, respond well to immunotherapy with checkpoint blockade therapy or the adoptive transfer of anti-tumor lymphocytes (43, 44). Therefore, we investigated whether BLM treatment improves the activation of autologous TILs in primary patient-derived bladder cancer cells. Firstly, we successfully established bladder cancer cells from patient tumor tissues and urine samples using a conditional reprogramming technique (45-47). In this study, eight patients diagnosed with bladder cancer were enrolled (Supplemental Table 5). Among these, four primary patient-derived cancer cell lines were established from the patient urine samples (BCC3, BCC16, BCC38, and BCC49), whereas the others were established from the tumor samples (BCC1, BCC15, BCC101, and BCC102). MHC-I expression could be induced by BLM in most of the primary patient-derived cancer cell lines with very low toxic effects (Supplemental Figure 15, A and B).

Among the four tumor samples, we selected BCC101 (high response) and BCC102 (low response) based on their response to BLM induced MHC-I expression. Subsequently, TILs from different fragments of the two tumor samples (labelled F1, F2, F3…) were expanded ex vivo and the phenotypes of the expended TILs were assessed by flow cytometry (Supplemental Figure 16, A-C). As expected, pre-treatment with BLM rendered BCC101 cells more susceptible to autologous TIL-mediated cytotoxicity than untreated cells, whereas BCC102 showed reduced effect (Figure 7G and Supplemental Figure 16D). We confirmed that BLM had no toxic effects to primary cancer cells within the range of experimental concentrations (Supplemental Figure 16E). Additionally, BLM pre-treated BCC101 cancer cells exhibited increased susceptibility to the cytotoxicity of autologous reactive TIL fractions, which was evidenced by a lower number of viable tumor cells, a higher apoptosis rate (Figure 7, H and I). Collectively, these results suggest that the potential of combination therapy with BLM rely on T cells as key effector cells, such as bispecific antibody, immune checkpoint therapy and TILs therapy for solid-tumor indications.

Discussion

Reduced surface expression of MHC-I stands as a formidable barrier to the success of immunotherapy. In this study, we present BLM as a promising agent, repurposed for its ability to rapidly induce surface MHC-I expression in tumor cells. This highlights MHC-I as an ideal pharmacological target for enhancing tumor immunity.

Utilizing a high-throughput flow cytometry system, we not only identified BLM but also demonstrated the versatility of our screening strategy to uncover potential immunotherapy-enhancing drugs. Moreover, the induction of downregulated MHC-I expression through BLM treatment presents a therapeutically valuable avenue to improve T cell anti-tumor immunity, overcoming obstacles posed by MHC-I expression limitations and opening possibilities for combination therapies.

BLM, traditionally an antibiotic chemotherapeutic agent with established use in various cancers, possesses anti-tumor activity attributed to its induction of specific double-strand DNA breaks (27, 39). Antigen processing and presentation in the MHC-I context is a complex, multi-step process subject to regulation at multiple levels (48). Previous studies have highlighted the involvement of the NF-κB and cGAS–STING pathways in cancer-related MHC-I expression (7, 49). Our results reveal that BLM treatment induces substantial DNA damage and promotes $CD8^+$ T cell activation through the specific upregulation of MHC-I expression in an ATM/ATR-NF-κB-dependent

manner. The dominant role of NF-κB in BLM-induced MHC-I upregulation reinforces the significance of the ATM/ATR-NF-κB pathway in regulating MHC-I expression in tumors. However, the specific molecular target of BLM remained unclear, and its identifying is crucial for a comprehensive understanding of its efficacy in MHC-I upregulation.

Building on BLM's induction of double-strand DNA breaks, the exploration of its synergy with DNA methyltransferase inhibitors in anti-tumor immunity emerges as a pivotal avenue. The experimental data presented in this study conclusively demonstrate that the combination therapy involving BLM and DNA methyltransferase inhibitors broadens the application potentials of both agents.

The importance of BLM in combination therapy becomes apparent as it showcases the potential to enhance various immunotherapy approaches that rely on T cells as primary effectors. This encompasses checkpoint blockade therapy, bispecific antibody therapy, and TILs therapy for solid tumor indications. The correlation established between high MHC-I expression and improved antigen presentation serves to validate the heightened efficacy of immunotherapies. Our study further establishes that BLM plays a crucial role in augmenting anti-tumor responses facilitated by these immunotherapy modalities.

Additionally, alternative pathways beyond MHC-I expression may contribute to the immune sensitivity of BLM-treated tumors, such as activated

IFN-α/γ and inflammatory pathways, which may facilitate T cell infiltration. Further research should delve into these alternative pathways to discern their impact on the immunological responsiveness of BLM-treated tumors.

Addressing pulmonary toxicity associated with BLM is imperative for its clinical application. While high doses (15 to 20 mg/kg) result in lung inflammation and pulmonary fibrosis (27, 50), our study indicates that a lower dosage of BLM (3 mg/kg) increases lymphocyte infiltration in tumor samples and remodels the tumor immune microenvironment without causing notable lung injury. This suggests the potential of repurposing BLM at lower doses, making it a more viable and economical option for cancer treatment.

TIL therapy represents an intricately personalized approach to cancer treatment, influenced by a multitude of variables and often yields unpredictable outcomes. Consequently, the inherent limitations of TIL therapy have spurred researchers to explore novel avenues for enhancing its efficacy. In this study, we reveal that BLM renders patient-derived bladder cancer cells more susceptible to cytotoxicity mediated by autologous TILs. This finding suggests a potential combination therapy to enhance the efficacy of TIL therapy.

This suppression of MHC-I is a critical viral strategy to avoid immune surveillance (51). The downregulation of MHC-I expression induced by Influenza A and B virus, which hinder viral clearance by $CD8^+$ T cells (52). SARS-CoV-2 can inhibit the induction of the MHC class I pathway by targeting

592 the STAT1-IRF1-NLRC5 axis (53). Restoring antigen presentation by
593 Interferon gamma can enhance the immune system's ability to combat viral
594 escape (54). BLM' s ability to induce MHC-I expression could, therefore,
595 provide a dual therapeutic strategy, augmenting the immune response against
596 both cancer cells and virally infected cells, making it a promising candidate for
597 further antiviral research. Interestingly, BLM has been reported to inhibit
598 multiple virus including HIV, picornavirus, herpesvirus, and poxvirus (55, 56).
599 This highlights the potential of BLM as an antiviral agent by combating
600 immune evasion. In summary, our data underscores the ability of BLM to
601 augment cytotoxic T cell recognition and responses by inducing surface MHC-
602 I expression in tumor cells. Furthermore, the potential of combination therapy
603 with BLM extends beyond adoptive T cell transfer therapy, encompassing
604 other immunotherapy modalities dependent on T cells as primary effectors.
605 The demonstrated correlation between MHC-I expression and improved
606 immunotherapy efficacy repurposes BLM as a key player in advancing the
607 field of cancer immunotherapy.
608

Methods

Additional details for methods are provided in the Supplemental Methods.

Sex as a biological variable

The mechanisms and pathways investigated are not sex-specific in our study. Female mice (C57BL/6) were exclusively used in the animal experiment due to their more docile nature, which leads to more consistent experimental conditions.

High-throughput flow cytometry screening system

To facilitate high-throughput screening, SU-DHL-4 cells were seeded in round-bottom 96-well plates and FDA-approved drugs were introduced into the cell plates. Additionally, each plate received 500 U/mL Interferon-γ (IFN-γ) (#315-05-20ug, PeproTech) and DMSO for the manual addition of positive and negative controls. After 48 h, the cells were labeled with the anti-HLA-A/B/C antibody W6/32-APC (#311410, BioLegend) at 4°C for 30 min. Subsequently, the cell samples were analyzed using the IntelliCyt iQue Screener PLUS (Sartorius).

Peptide Pulsing Assay

For the peptide pulsing assay, B16F10 cells were pre-treated with BLM at

630 the indicated concentrations or with PBS as a control for specified durations.
631 Following this treatment, the cells were pulsed with 1 ng/mL of SIINFEKL
632 (Ovalbumin peptide, OVA peptide) at 37°C for 2 h. The cell surface
633 expression of H-2K^{b}-SIINFEKL was assessed using flow cytometry. In the co-
634 culture experiments, the culture media were removed, and the cells were
635 washed with PBS to eliminate residual BLM and OVA peptide after pulsing.
636 Subsequently, OT-I CD8^{+} T cells were added at a 2:1 effector to target (E/T)
637 ratio. After approximately 20 h of co-culture, all cells were harvested and
638 analyzed using flow cytometry. Tumor cells were identified as the CD45-
639 negative population, and the cell apoptosis rate was determined using the
640 Annexin V/633 Apoptosis Detection Kit (AD11, DOJINDO, Japan) and
641 analyzed with FlowJo™ v10.7 Software (BD Life Sciences, USA).
642

643 **Co-culture of cancer cells and T cells for T cell cytotoxicity assay**

644 *Co-culture of mouse tumor cells and OT-I CD8^{+} T cells.* C57BL/6-Tg
645 (TcraTcrb)1100Mjb/J (OT-I) mice were generously shared by Jianhua Li' s lab
646 from the Department of Pathogen Biology at School of Basic Medical
647 Sciences, Fudan University, Shanghai. B16F10 and B16OVA cells were pre-
648 treatment with BLM (1.25 μM or 2.5 μM, respectively) or PBS for 24 h. CD8^{+} T
649 cells were isolated from the spleens and lymph nodes of OT-I mice,
650 stimulated with SIINFEKL (OVA peptide) (#HY-P1489A, InvivoGen), and
651 cultured in RPMI 1640 medium containing 10% FBS, 1% penicillin-

streptomycin, 2 mM L-glutamine (#25030081, Gibco, Thermo Fisher), 10 mM HEPES (#15630080, Gibco, Thermo Fisher), MEM NEAA (#11140050, Gibco, Thermo Fisher), 50 μM β-Mercaptoethanol (#444203, Sigma), and 10 ng/mL recombinant mouse IL-2 (#78081, STEMCELL, Canada). These mouse $CD8^+$ T cells were then co-cultured with BLM- or PBS pre-treated tumor cells at a ratio of 1:2 (tumor cells: T cells) for approximately 20 h. At the conclusion of the experiment, the concentration of IFN-γ in the co-culture supernatant was determined by ELISA, and the percentage of apoptotic tumor cells was assessed by flow cytometry.

Co-culture of human tumor cells and human $CD8^+$ T cells (Bispecific antibody treament). SK-BR-3 cells were pre-treated with BLM (1.25 μM) or PBS for 24 h. Peripheral blood mononuclear cells (PBMCs) were collected from healthy donors with informed consent and isolated via density gradient centrifugation using Ficoll Paque Plus (GE Healthcare, 17144003). $CD8^+$ T cells were subsequently purified from PBMCs using negative selection with the EasySep Human $CD8^+$ T Cell Enrichment Kit (#19053, STEMCELL, Canada) following the manufacturer's protocol. Human $CD8^+$ T cells were stimulated in 12-well culture plates coated with 1 μg/mL anti-human CD3 antibody (#300402, BioLegend) and 2 μg/mL soluble anti-human CD28 antibody (#302902, BioLegend) along 10 ng/mL recombinant human IL-2 (#200-02-1MG, PeproTech, Thermo Fisher). Human $CD8^+$ T cells were cultured in RPMI 1640 medium containing 10% FBS, 1% penicillin-streptomycin, 2 mM L-glutamine

(#25030081, Gibco, Thermo Fisher), 10 mM HEPES (#15630080, Gibco, Thermo Fisher), MEM NEAA (#11140050, Gibco, Thermo Fisher), and 50 μM β-Mercaptoethanol (#444203, Sigma). Co-culture experiments involving human $CD8^+$ T cells and BLM or PBS pre-treated tumor cells at a ratio of 1:2 (tumor cells: T cells) in the presence of the appropriate bispecific antibody (0.3 nM H2-scDb) for approximately 20 h. At the conclusion of the experiment, the concentration of IFN-γ in the co-culture supernatant was measured using ELISA.

Co-culture of NY-ESO-1^+ human tumor cells and human $CD8^+$ T cells transduced with the NY-ESO-1 TCR. Human $CD8^+$ T cells were engineered to express a recombinant T cell receptor (TCR) targeting the NY-ESO-1 antigen (specifically the NY-ESO-1:157–165 epitope) in an HLA-A*02-restricted fashion (referred to as ESO T cells). NY-ESO-1^+ SK-BR-3 cell was conducted by overexpressing NY-ESO-1 gene. NY-ESO-1^+ SK-BR-3 cells were pre-treated with BLM (2.5 μM, 5 μM, 10 μM, and 20 μM) or PBS for 24 h. ESO T cells were then co-cultured with BLM- or PBS pre-treated NY-ESO-1^+ SK-BR-3 cells at a ratio of 1:2 (tumor cells: T cells) for approximately 20 h. At the conclusion of the experiment, the percentage of apoptotic tumor cells was assessed by flow cytometry.

Bispecific antibody production

Bispecific antibody production was performed as previously described

(41). Briefly, 1 L FreeStyle 293-F cells were transfected with 1.2 mg of plasmid DNA using polyethylenimine (PEI). After three days, the culture medium was collected and filtered through a 0.45-μm filter. Ni-NTA Agarose (#30210, QIAGEN) was pre-equilibrated with PBS and incubated overnight with the supernatant. Following this, non-specifically bound proteins were removed from the agarose by washing with PBS, 10 mM, and 20 mM imidazole before being eluted with 50 mM and 100 mM imidazole. The protein was concentrated and desalted in PBS using Amicon Ultra-15 Centrifugal Filters (#UFC901096, Sigma-Aldrich). The protein concentration was determined using Coomassie blue staining and/or the Pierce BCA Protein Assay Kit (#23225, Thermo Scientific).

Adoptive T Cell Transfer Therapy and BrdU labeling

B16OVA cells (2×10^5/mouse) were subcutaneously injected into the right flank of C57BL/6 mice (purchased from Shanghai JieSiJie Laboratory Animal Company Limited, 6-8 weeks old). After eight days, when the tumor volume reached ~100 mm^3, the mice were randomly assigned to different treatment groups and received either PBS or BLM (3 mg/kg, dissolved in PBS). Tumor size was monitored every two days. On the 11th day, pre-activated OT-I $CD45.1^+$ cells (1×10^6/mouse) were intravenously injected into tumor-bearing mice. For in vivo BrdU labeling of transferred OT-I cells, mice were injected intraperitoneally with 1 mg (0.1 mg/mL) of BrdU (BD Bioscience) in 1× PBS 24

718 and 48 h after OT-I transfer. Tumors were harvested and BrdU staining kit
719 was used for the flow cytometry analysis 72 h after OT-I transfer. For tumor
720 weight and lung toxicity evaluation, all tumor-bearing mice were humanely
721 euthanized and their tumors and lungs were collected on the 18^{th} day. For
722 survival studies, endpoints included death, mouse weight loss exceeding 20%,
723 significant tumor ulceration, and tumor volume exceeding 2000 mm^3. Animal
724 survival rates were recorded daily.
725
726 **Expansion of TILs and tumor cell lines from patient-derived bladder**
727 **tumor samples**
728 Fresh tumor samples were sectioned into small fragments measuring
729 approximately 1-3 mm^3, which were then placed into a culture medium
730 containing 60,000 IU/mL of IL-2. After four weeks of expansion, the resulting
731 TILs were either cryopreserved or subjected to a rapid expansion protocol
732 (REP) involving irradiated human PBMCs as feeder cells. Bladder tumor cell
733 lines were established according to previously established protocols (47).
734 The established bladder tumor cells were pretreatment with BLM or were
735 exposed to PBS for 24 h. Simultaneously, expanded TILs were harvested
736 post-REP and co-cultured with BLM pre-treated or PBS-exposed tumor cells
737 at a ratio of 1:4 (tumor cells : TILs) for approximately 20 h. Cytotoxicity was
738 assessed using CellTiter-Glo reagent (Promega), and the concentration of
739 IFN-γ in the co-culture supernatant was determined by ELISA.

Statistical Analysis

Data are represented as mean ± SEM. Differences between two groups and among multiple groups were evaluated using a two-tailed Student's t-test and one-way ANOVA, respectively. Each experiment was repeated three times independently. Data analyses were conducted using the SPSS software (SPSS, Chicago, IL, USA). A *P* value less than 0.05 was considered significant.

Study approval:

This study enrolled eight patients diagnosed with bladder cancer, with four having high-grade and four with low-grade forms of the disease. The detailed clinical information of the patients is listed in Supplemental Table 7. All experimental procedures were approved by the Zhongshan Hospital Ethics Committee (project numbers: B2016-148 and B2017-129R) and Medical Ethics Committee of the School of Basic Medical Sciences, Fudan University (project number: 2023-C005). Informed consent was obtained from all the patients. All animal experiments were performed based on the guidelines published by the Association for Assessment and Accreditation of Laboratory Animal Care, and the animal studies were approved by the Department of Laboratory Animal Science Fudan University.

Data availability:

762 The single-cell RNA-sequencing data and the bulk RNA-sequencing data
763 in this study have been deposited in CNGB Nucleotide Sequence Archive of
764 China National GeneBank (https://db.cngb.org/cnsa/). The accession
765 numbers are CRA017507 and HRA007881, respectively. Values for all data
766 points found in graphs are in the Supporting Data Values file.
767
768 **Authors' contributions:** Y.J.D., W.J. and W.X. conceived and supervised the
769 project; Q.Y., Y.D., X.B.W. and C.X.S. conducted the experiments; S.J., Y.D.,
770 C.X.S., and R.K.Z. provided biopsy samples and cultured primary cells and
771 TILs; Q.Y. analyzed the data; Q.Y. wrote the manuscript; and Y.J.D. and W.J.
772 modified the manuscript. All the authors have read and approved the final
773 manuscript.
774
775 **Acknowledgements:** We thank support from prof. Jianhua Li from Fudan
776 University. This work was supported by the National Key Research and
777 Development Program of China (No.2022YFC2804800 to W.J.), the National
778 Natural Science Foundation of China (No. 22137002, 21877016 to Y.D.,
779 92253305, 82273021, 81972621 to W.J., and No. 82073413 to S.J.), the
780 Science and Technology Commission of Shanghai Municipality (Grant
781 20JC1410900 to Y.D.), the University Innovation Research Group in
782 Chongqing (No. CXQT21016 to Y.D.), the Chongqing Talent Program Project
783 (No. CQYC20200302119 to Y.D.), High-Level Innovation Platform Cultivation

784 Plan of Chongqing (to Y.D.), Joint Fund of the Natural Science Innovation and
785 Development Foundation of Chongqing (to Y.D.), and Program for Professor
786 of Special Appointment (Eastern Scholar) at Shanghai Institutions of Higher
787 Learning (to W.J.).
788

References

1. Le DT, Durham JN, Smith KN, Wang H, Bartlett BR, Aulakh LK, et al. Mismatch repair deficiency predicts response of solid tumors to PD-1 blockade. *Science (New York, NY).* 2017;357(6349):409-13.

2. Sharma P, Hu-Lieskovan S, Wargo JA, and Ribas A. Primary, Adaptive, and Acquired Resistance to Cancer Immunotherapy. *Cell.* 2017;168(4):707-23.

3. Torphy RJ, Sun Y, Lin R, Caffrey-Carr A, Fujiwara Y, Ho F, et al. GPR182 limits antitumor immunity via chemokine scavenging in mouse melanoma models. *Nature communications.* 2022;13(1):97.

4. Ruiz-Cabello F, and Garrido F. HLA and cancer: from research to clinical impact. *Immunology today.* 1998;19(12):539-42.

5. Ruiz-Cabello F, Cabrera T, Lopez-Nevot MA, and Garrido F. Impaired surface antigen presentation in tumors: implications for T cell-based immunotherapy. *Seminars in cancer biology.* 2002;12(1):15-24.

6. Garrido F. MHC Class-I Loss and Cancer Immune Escape Introduction. *Advances in Experimental Medicine and Biology.* 2019(1151-):1151.

7. Cornel AM, Mimpen IL, and Nierkens S. MHC Class I Downregulation in Cancer: Underlying Mechanisms and Potential Targets for Cancer Immunotherapy. *Cancers.* 2020;12(7).

8. Taylor BC, Sun X, Gonzalez-Ericsson PI, Sanchez V, Sanders ME, Wescott EC, et al. NKG2A is a Therapeutic Vulnerability in Immunotherapy Resistant MHC-I Heterogeneous Triple Negative Breast Cancer. *Cancer discovery.* 2023.

9. Na HY, Park Y, Nam SK, Lee KS, Oh HK, Kim DW, et al. Expression of human leukocyte antigen class I and β2-microglobulin in colorectal cancer and its prognostic impact. *Cancer science.* 2021;112(1):91-100.

10. Roemer MG, Advani RH, Redd RA, Pinkus GS, Natkunam Y, Ligon AH, et al. Classical Hodgkin Lymphoma with Reduced β2M/MHC Class I Expression Is Associated with Inferior Outcome Independent of 9p24.1 Status. *Cancer immunology research.* 2016;4(11):910-6.

11. Datar IJ, Hauc SC, Desai S, Gianino N, Henick B, Liu Y, et al. Spatial Analysis and Clinical Significance of HLA Class-I and Class-II Subunit Expression in Non-Small Cell Lung Cancer. *Clinical cancer research : an official journal of the American Association for Cancer Research.* 2021;27(10):2837-47.

12. Romero JM, Jiménez P, Cabrera T, Cózar JM, Pedrinaci S, Tallada M, et al. Coordinated downregulation of the antigen presentation machinery and HLA class

824 I/beta2-microglobulin complex is responsible for HLA-ABC loss in bladder cancer.
825 *International journal of cancer.* 2005;113(4):605-10.

826 13. Kawase K, Kawashima S, Nagasaki J, Inozume T, Tanji E, Kawazu M, et al. High
827 Expression of MHC Class I Overcomes Cancer Immunotherapy Resistance Due to IFNγ
828 Signaling Pathway Defects. *Cancer immunology research.* 2023;11(7):895-908.

829 14. LaFleur MW, and Sharpe AH. CRISPR Screens to Identify Regulators of Tumor
830 Immunity. *Annual review of cancer biology.* 2022;6:103-22.

831 15. Taylor BC, and Balko JM. Mechanisms of MHC-I Downregulation and Role in
832 Immunotherapy Response. *Frontiers in immunology.* 2022;13:844866.

833 16. Goel S, DeCristo MJ, Watt AC, BrinJones H, Sceneay J, Li BB, et al. CDK4/6 inhibition
834 triggers anti-tumour immunity. *Nature.* 2017;548(7668):471-5.

835 17. Dersh D, Phelan JD, Gumina ME, Wang B, Arbuckle JH, Holly J, et al. Genome-wide
836 Screens Identify Lineage- and Tumor-Specific Genes Modulating MHC-I- and MHC-II-
837 Restricted Immunosurveillance of Human Lymphomas. *Immunity.* 2021;54(1):116-31.e10.

838 18. Jongsma MLM, Guarda G, and Spaapen RM. The regulatory network behind MHC class
839 I expression. *Molecular immunology.* 2019;113:16-21.

840 19. Jimi E, Strickland I, Voll RE, Long M, and Ghosh S. Differential role of the transcription
841 factor NF-kappaB in selection and survival of CD4+ and CD8+ thymocytes. *Immunity.*
842 2008;29(4):523-37.

843 20. Zhou Y, Bastian IN, Long MD, Dow M, Li W, Liu T, et al. Activation of NF-κB and
844 p300/CBP potentiates cancer chemoimmunotherapy through induction of MHC-I antigen
845 presentation. *Proceedings of the National Academy of Sciences of the United States of*
846 *America.* 2021;118(8).

847 21. Kalbasi A, Tariveranmoshabad M, Hakimi K, Kremer S, Campbell KM, Funes JM, et al.
848 Uncoupling interferon signaling and antigen presentation to overcome immunotherapy
849 resistance due to JAK1 loss in melanoma. *Science translational medicine.* 2020;12(565).

850 22. Schmudde M, Braun A, Pende D, Sonnemann J, Klier U, Beck JF, et al. Histone
851 deacetylase inhibitors sensitize tumour cells for cytotoxic effects of natural killer cells.
852 *Cancer letters.* 2008;272(1):110-21.

853 23. Hicks KC, Fantini M, Donahue RN, Schwab A, Knudson KM, Tritsch SR, et al.
854 Epigenetic priming of both tumor and NK cells augments antibody-dependent cellular
855 cytotoxicity elicited by the anti-PD-L1 antibody avelumab against multiple carcinoma cell
856 types. *Oncoimmunology.* 2018;7(11):e1466018.

857 24. Gameiro SR, Malamas AS, Tsang KY, Ferrone S, and Hodge JW. Inhibitors of histone
858 deacetylase 1 reverse the immune evasion phenotype to enhance T-cell mediated lysis of

prostate and breast carcinoma cells. *Oncotarget.* 2016;7(7):7390-402.

25. Patel SJ, Sanjana NE, Kishton RJ, Eidizadeh A, Vodnala SK, Cam M, et al. Identification of essential genes for cancer immunotherapy. *Nature.* 2017;548(7669):537-42.

26. Matsushima S, Ajiro M, Iida K, Chamoto K, Honjo T, and Hagiwara M. Chemical induction of splice-neoantigens attenuates tumor growth in a preclinical model of colorectal cancer. *Science translational medicine.* 2022;14(673):eabn6056.

27. Burgy O, Wettstein G, Bellaye PS, Decologne N, Racoeur C, Goirand F, et al. Deglycosylated bleomycin has the antitumor activity of bleomycin without pulmonary toxicity. *Science translational medicine.* 2016;8(326):326ra20.

28. Gulati GS, Sikandar SS, Wesche DJ, Manjunath A, Bharadwaj A, Berger MJ, et al. Single-cell transcriptional diversity is a hallmark of developmental potential. *Science (New York, NY).* 2020;367(6476):405-11.

29. Qin Q, Fan J, Zheng R, Wan C, Mei S, Wu Q, et al. Lisa: inferring transcriptional regulators through integrative modeling of public chromatin accessibility and ChIP-seq data. *Genome biology.* 2020;21(1):32.

30. Dhatchinamoorthy K, Colbert JD, and Rock KL. Cancer Immune Evasion Through Loss of MHC Class I Antigen Presentation. *Frontiers in immunology.* 2021;12:636568.

31. Burr ML, Sparbier CE, Chan KL, Chan YC, Kersbergen A, Lam EYN, et al. An Evolutionarily Conserved Function of Polycomb Silences the MHC Class I Antigen Presentation Pathway and Enables Immune Evasion in Cancer. *Cancer cell.* 2019;36(4):385-401.e8.

32. Ferrari V, Lo Cascio A, Melacarne A, Tanasković N, Mozzarelli AM, Tiraboschi L, et al. Sensitizing cancer cells to immune checkpoint inhibitors by microbiota-mediated upregulation of HLA class I. *Cancer cell.* 2023;41(10):1717-30.e4.

33. Bolzán AD, and Bianchi MS. DNA and chromosome damage induced by bleomycin in mammalian cells: An update. *Mutation research Reviews in mutation research.* 2018;775:51-62.

34. Harding SM, Benci JL, Irianto J, Discher DE, Minn AJ, and Greenberg RA. Mitotic progression following DNA damage enables pattern recognition within micronuclei. *Nature.* 2017;548(7668):466-70.

35. Mackenzie KJ, Carroll P, Martin CA, Murina O, Fluteau A, Simpson DJ, et al. cGAS surveillance of micronuclei links genome instability to innate immunity. *Nature.* 2017;548(7668):461-5.

36. Khosravi R, Maya R, Gottlieb T, Oren M, Shiloh Y, and Shkedy D. Rapid ATM-dependent phosphorylation of MDM2 precedes p53 accumulation in response to DNA

damage. *Proceedings of the National Academy of Sciences of the United States of America.* 1999;96(26):14973-7.

37. Mishra A, Doyle NA, and Martin WJc. Bleomycin-mediated pulmonary toxicity: evidence for a p53-mediated response. *American journal of respiratory cell and molecular biology.* 2000;22(5):543-9.

38. Jorgovanovic D, Song M, Wang L, and Zhang Y. Roles of IFN-γ in tumor progression and regression: a review. *Biomarker research.* 2020;8:49.

39. Roy B, Tang C, Alam MP, and Hecht SM. DNA methylation reduces binding and cleavage by bleomycin. *Biochemistry.* 2014;53(38):6103-12.

40. Maes K, De Smedt E, Lemaire M, De Raeve H, Menu E, Van Valckenborgh E, et al. The role of DNA damage and repair in decitabine-mediated apoptosis in multiple myeloma. *Oncotarget.* 2014;5(10):3115-29.

41. Hsiue EH, Wright KM, Douglass J, Hwang MS, Mog BJ, Pearlman AH, et al. Targeting a neoantigen derived from a common TP53 mutation. *Science (New York, NY).* 2021;371(6533).

42. Kumar S, Zeng Z, Bagati A, Tay RE, Sanz LA, Hartono SR, et al. CARM1 Inhibition Enables Immunotherapy of Resistant Tumors by Dual Action on Tumor Cells and T Cells. *Cancer discovery.* 2021;11(8):2050-71.

43. Dolton G, Rius C, Wall A, Szomolay B, Bianchi V, Galloway SAE, et al. Targeting of multiple tumor-associated antigens by individual T cell r eceptors during successful cancer immunotherapy. *Cell.*186(16):3333-49.e27.

44. Zacharakis N, Chinnasamy H, Black M, Xu H, Lu YC, Zheng Z, et al. Immune recognition of somatic mutations leading to complete durable regression in metastatic breast cancer. *Nature medicine.* 2018;24(6):724-30.

45. Wang Z, Li Y, Zhao W, Jiang S, Huang Y, Hou J, et al. Integrative multi-omics and drug-response characterization of patient-derived prostate cancer primary cells. *Signal transduction and targeted therapy.* 2023;8(1):175.

46. Wang J, Zhu J, Hu J, Wang Z, Wang X, Pan J, et al. A novel in vitro prognostic model of bladder cancer based on urine-derived living tumor cells. *Genes & diseases.* 2023;10(6):2586-96.

47. Jiang S, Wang J, Yang C, Tan R, Hou J, Shi Y, et al. Continuous culture of urine-derived bladder cancer cells for precision medicine. *Protein & cell.* 2019;10(12):902-7.

48. Leone P, Shin EC, Perosa F, Vacca A, Dammacco F, and Racanelli V. MHC class I antigen processing and presenting machinery: organization, function, and defects in tumor cells. *Journal of the National Cancer Institute.* 2013;105(16):1172-87.

49. Gu SS, Zhang W, Wang X, Jiang P, Traugh N, Li Z, et al. Therapeutically Increasing MHC-I Expression Potentiates Immune Checkpoint Blockade. *Cancer discovery.* 2021;11(6):1524-41.

50. Liu T, De Los Santos FG, and Phan SH. The Bleomycin Model of Pulmonary Fibrosis. *Methods in molecular biology (Clifton, NJ).* 2017;1627:27-42.

51. van de Weijer ML, Luteijn RD, and Wiertz EJ. Viral immune evasion: Lessons in MHC class I antigen presentation. *Seminars in immunology.* 2015;27(2):125-37.

52. Koutsakos M, McWilliam HEG, Aktepe TE, Fritzlar S, Illing PT, Mifsud NA, et al. Downregulation of MHC Class I Expression by Influenza A and B Viruses. *Frontiers in immunology.* 2019;10:1158.

53. Yoo JS, Sasaki M, Cho SX, Kasuga Y, Zhu B, Ouda R, et al. SARS-CoV-2 inhibits induction of the MHC class I pathway by targeting the STAT1-IRF1-NLRC5 axis. *Nature communications.* 2021;12(1):6602.

54. Hengel H, Lucin P, Jonjić S, Ruppert T, and Koszinowski UH. Restoration of cytomegalovirus antigen presentation by gamma interferon combats viral escape. *Journal of virology.* 1994;68(1):289-97.

55. Georgiou NA, van der Bruggen T, Healy DM, van Tienen C, de Bie P, Oudshoorn M, et al. Bleomycin has antiviral properties against drug-resistant HIV strains and sensitises virus to currently used antiviral agents. *International journal of antimicrobial agents.* 2006;27(1):63-8.

56. Nørskov-Lauritsen N, and Ebbesen P. Bleomycin differentially inhibits picornavirus, herpesvirus and poxvirus replication in a human carcinoma cell line. *In vivo (Athens, Greece).* 1993;7(6a):481-5.

Figures and figure legends

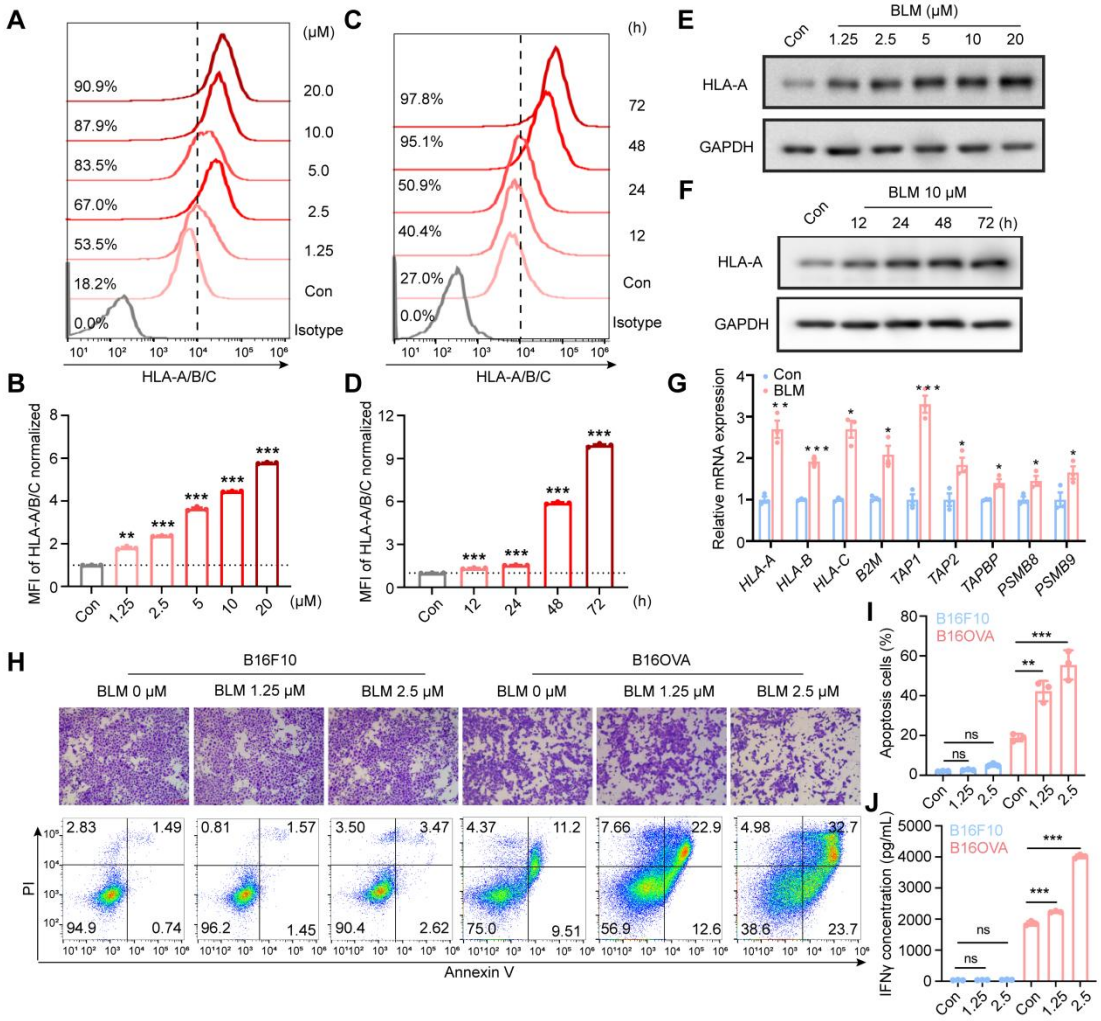

Figure 1. BLM-mediated increasing of MHC-I expression primes CD8⁺ T cell activation. (**A**) Cell surface HLA-A/B/C in SU-DHL-4 cells after incubation with the indicated concentrations of BLM for 48 h. (**B**) Quantification of mean fluorescence intensities (MFI) of HLA-A/B/C from (**A**), n=3 per group. (**C**) Cell surface HLA-A/B/C in SU-DHL-4 cells following incubation with 10 μM BLM for 12, 24, 48, and 72 h. (**D**) Quantification of MFI of HLA-A/B/C from (**C**), n=3 per group. (**E** and **F**) Western blot analysis of the HLA-A expression in SU-DHL-4 cells after the indicated BLM concentrations in (**E**) or BLM treatment times in (**F**). (**G**) qRT-PCR analysis of the antigen

presentation gene expression in SU-DHL-4 cells after BLM treatment for 48 h. (**H**) Co-culture of murine cancer cells and OT-I T cells for T cell cytotoxicity assay. B16F10 or B16OVA cells were pre-treated with indicated concentrations of BLM for 24 h prior to co-culture with OT-I T cells. The first lane displays the crystal violet staining images of remaining cancer cells (Scale bars, 400 μm). The second lane presents the representative images of cancer cells apoptosis after co-culture with OT-I T cells. (**I**) Quantification of the percentages of early and late apoptotic cells among cancer cells from (**H**), n=3 per group. (**J**) The concentration of IFN-γ in the co-culture supernatant as detected by ELISA, n=3 per group. Student's two-tailed unpaired t test, $*P < 0.05$, $**P < 0.01$ and $***P < 0.001$ compared to the vehicle group; ns, no significance. Data indicate the mean ± SD. $*P < 0.05$, $**P < 0.01$, $***P < 0.001$, and ns, no significance compared to the vehicle group by one-way ANOVA (**B**, **D**, **I**, and **J**) and unpaired t test (**G**).

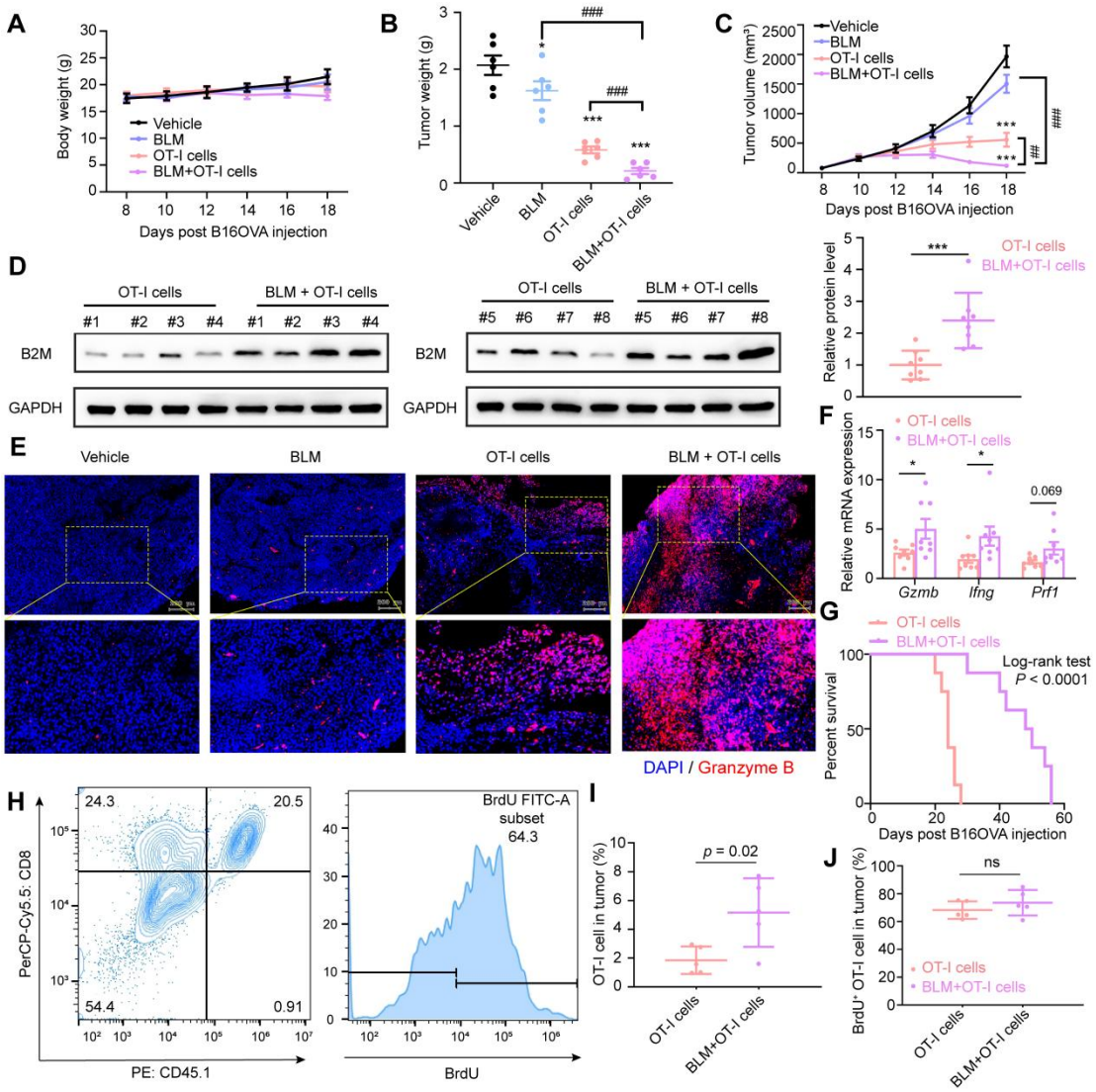

Figure 2. Potentiated anti-tumor response of T cells by BLM treatment. (**A**) Experimental procedure for the adoptive T cell transfer. (**B**-**D**) Mice body weight (**B**), tumor weight (**C**), and tumor volume (**D**), n=8 per group. (**E**) Western blot analysis of B2M level in tumor tissues as indicated. (**F**) Mouse melanoma tissues were stained for Granzyme B (red) together with DAPI (blue) (Scale bars, 200 μm). (**G**) RT-PCR analysis of gene expression of anti-tumor effector molecules including granzyme B (*Gzmb*), IFN-γ (*Ifng*), and perforin (*Prf1*) in tumor tissues. (**H**) Kaplan–Meier curves for B16OVA tumor bearing mice treated with OT-I cells or with the combination treatment of OT-I

989 cells and BLM. (**I**) Representative flow cytometry plot of transferred OT-I T
990 cells ($CD45.1^+CD8^+$) and BrdU staining. (**J** and **K**) Three days after transfer,
991 the frequencies of transferred OT-I cells ($CD45.1^+CD8^+$) (**J**) and $BrdU^+$ OT-I
992 cells (**K**) were quantified in tumors from B16OVA mice pretreated by BLM or
993 not, n=5 per group. Data are shown as mean ± SD. *P < 0.05, **P < 0.01, ***P
994 < 0.001, and ns, no significance compared to the vehicle group by one-way
995 ANOVA (**C** and **D**) and unpaired t test (**E**, **G**, **J**, and **K**); #P < 0.05, ##P < 0.01
996 and ###P < 0.001 between the indicated groups by unpaired t test (**C** and **D**).
997

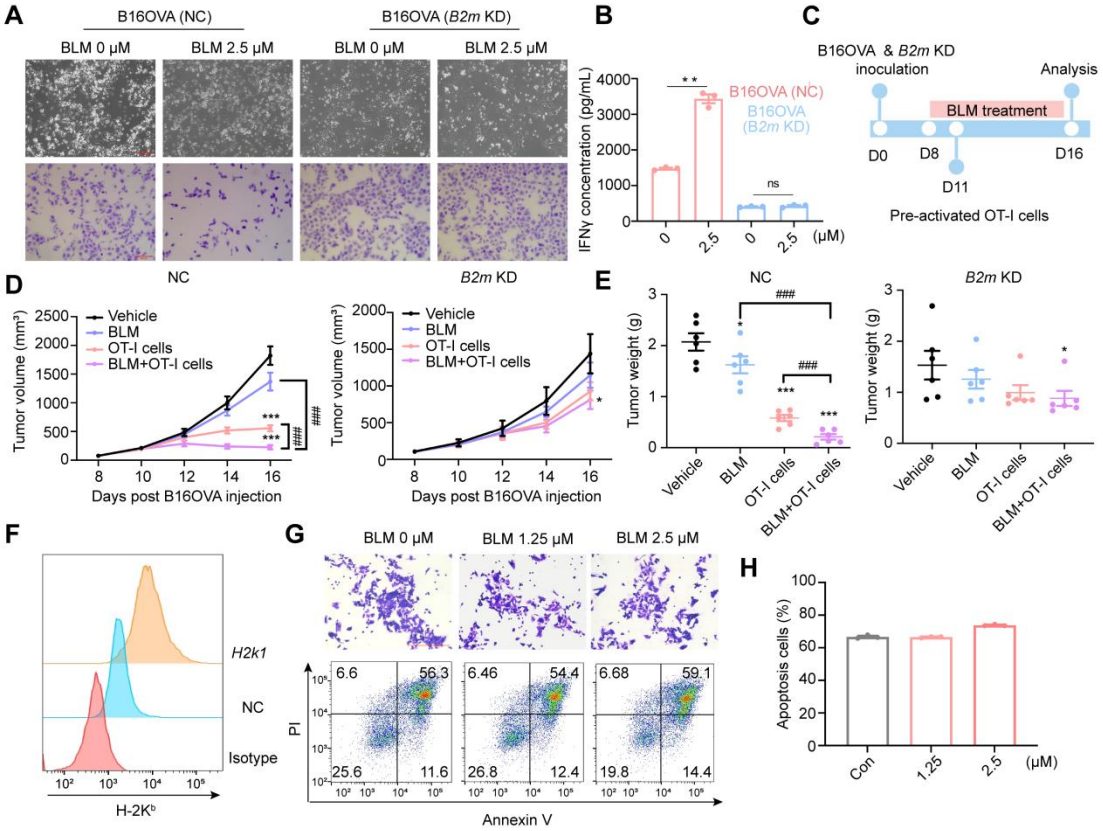

998

999 **Figure 3. MHC-I in cancer cells is indispensable for the anti-tumor effect**

1000 **of BLM.** (**A**) Co-culture of non-targeting control (NC) or *B2m* knockdown

1001 B16OVA cells and OT-I T cells for T cell cytotoxicity assay. Cells were pre-

1002 treated with indicated concentrations of BLM for 24 h prior to co-culture with

1003 OT-I T cells. The first lane shows the microscopy images and the second lane

1004 displays the crystal violet staining images (Scale bars, 400 μm). (**B**)

1005 Concentration of IFN-γ in the co-culture supernatant as detected by ELISA,

1006 n=3 per group. (**C-E**) The experimental procedure (**C**), tumor volumes (**D**),

1007 and tumor weights (**E**) on day 16, n=6 per group. (**F**) Flow cytometry detected

1008 cell surface H-2K^{b} expression in non-targeting control (NC) or *H2k1*

1009 overexpressing B16OVA cells. (**G**) Co-culture of B16OVA cells

1010 overexpressing *H2k1* and OT-I T cells for T cell cytotoxicity assay. B16OVA

cells overexpressing *H2k1* were pre-treated with indicated concentrations of BLM for 24 h prior to co-culture with OT-I T cells. The first lane displays the crystal violet staining images of remaining cancer cells (Scale bars, 400 μm). The second lane presents the representative images of cancer cells apoptosis after co-culture with OT-I T cells. (**H**) Quantification of the percentages of early and late apoptotic cells among cancer cells from (**G**), n=3 per group. Data are shown as mean ± SD. **P* < 0.05, ***P* < 0.01, ****P* < 0.001, and ns, no significance compared to the vehicle group by unpaired t test (**B**) and one-way ANOVA (**D** and **E**); ###*P* < 0.001 between the indicated groups by unpaired t test (**D** and **E**).

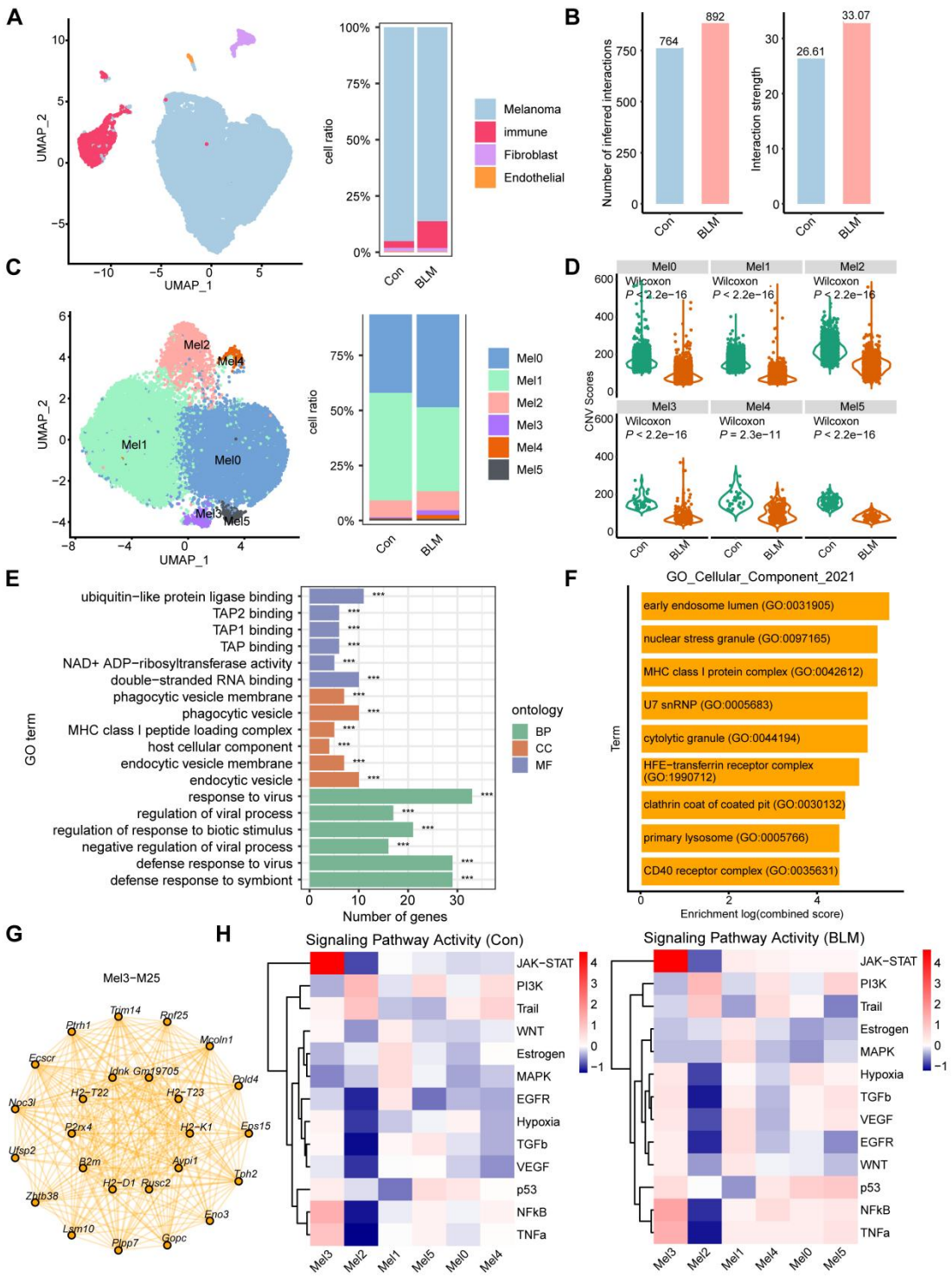

Figure 4. BLM treatment remodels the tumor microenvironment. (**A**) UMAP based on the top 20 principal components of all single-cell transcriptomes color-coded by main cell type, and proportion of main cell type per tumor sample. (**B**) The number of inferred interactions and interaction

strength were computed by CellChat package among control (Con) and BLM tumor samples. (**C**) U-MAP based on the top 20 principal components of all single-cell transcriptomes color-coded by melanoma subclusters, and proportion of melanoma subclusters per tumor sample. (**D**) CNV scores among melanoma subclusters (Mel0-Mel5) in different groups were computed by infercnv package. (**E**) GO function enrichment analysis for melanoma subcluster three (Mel3) was determined by clusterProfiler package. (**F**) The gene set functional analyses of module25 were conducted with enrichR package. (**G**) Network plot visualized the network underlying the top 25 hub genes for module25. (**H**) Mean pathway activity scores of melanoma tumor cells among different subclusters in control (Con) and BLM groups. ***$P <$ 0.001.

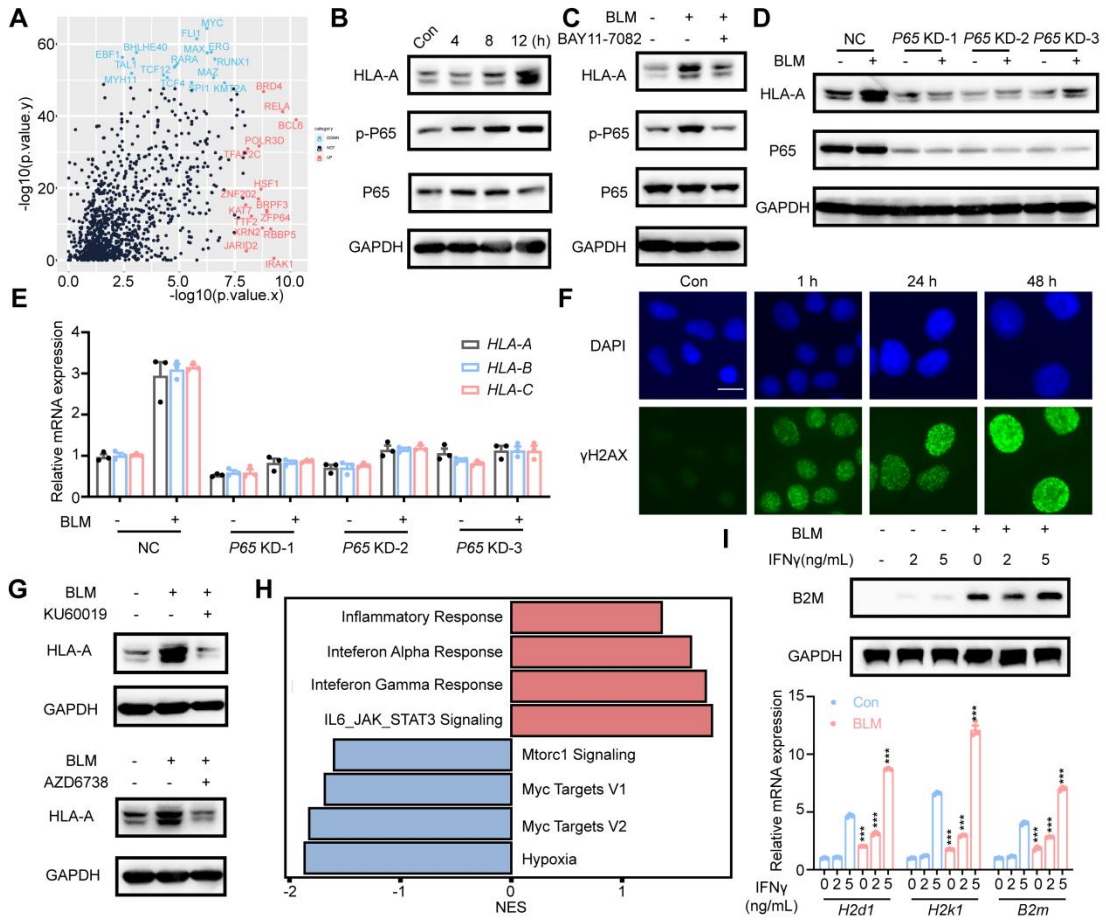

Figure 5. MHC-I upregulation caused by BLM depends on ATM/ATR-NF-κB activation. (**A**) DEGs identified in comparisons of BLM-treated cells relative to control were subjected to LISA. The top 30 enriched regulators of up-regulated (red) and down-regulated (blue) DEGs were noted. (**B**) Western blot analysis of indicated proteins in SK-BR-3 cells treated with 10 μM BLM for the indicated times. (**C**) Western blot analysis of the HLA-A, p-P65, and P65 expressions. SK-BR-3 cells were pre-treated with 5 μM BAY11-7082 for 6 h, then followed by 10 μM BLM for 12 h. (**D**) HLA-A protein levels examined in *P65*-depleted SK-BR-3 cells 48 h after BLM treatment. (**E**) qRT-PCR analysis of gene expressions of HLA-A, HLA-B, and HLA-C in *P65*-depleted SK-BR-3 cells 48 h after BLM treatment. (**F**) Immunofluorescence analysis of dsDNA

damage by γH2AX S139 antibody staining (Green foci; nuclei labeled with DAPI) in SK-BR-3 cells after the indicated times of BLM treated (Scale bars, 25 μm). (**G**) Western blot analysis of the HLA-A expression in SK-BR-3 cells. Cells were pre-treated with 10 μM KU60019 or 10 μM AZD6738, for 6 h, then followed with 10 μM BLM for 12 h. (**H**) Gene Set Enrichment Analysis (GSEA) analysis of significantly upregulated/downregulated pathways in BLM treatment versus control SK-BR-3 cells. (**I**) Western blot and qRT-PCR analysis of MHC-I expression levels in B16F10 cells after BLM treatment in the presence of 2 or 5 ng/mL IFN-γ for 48 h. Data are shown as mean ± SD. ***$P < 0.001$ compared to the vehicle group by one-way ANOVA.

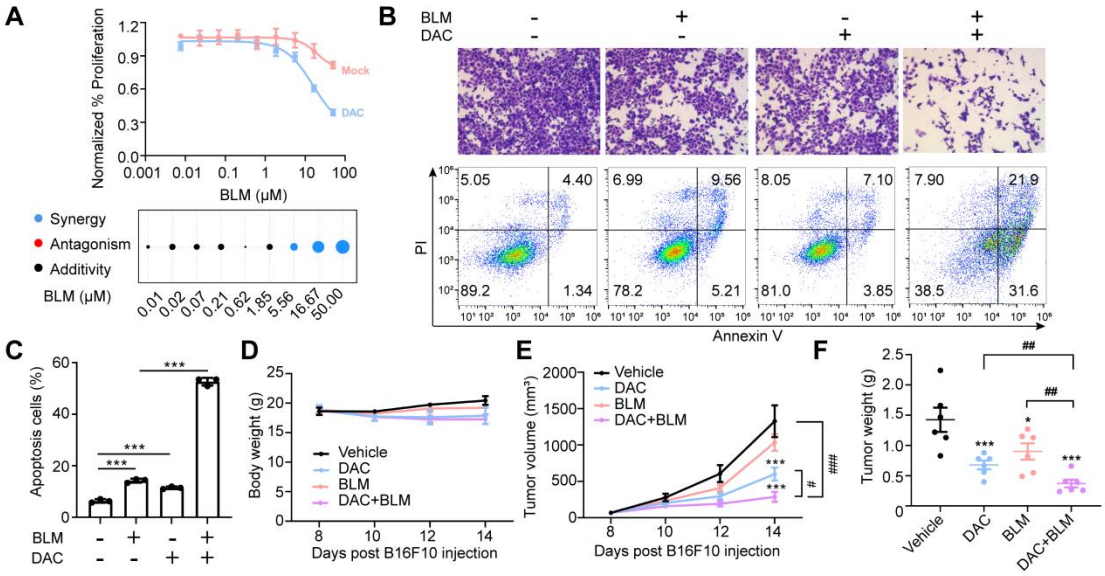

Figure 6. DNA methyltransferase inhibition promotes BLM-induced anti-tumor immune responses. (**A**) Top panel: Growth inhibition as detected by cell viability of SK-BR-3 cells treated with mock/100 nM DAC for five days and BLM for two days. Bottom panel: Combination index (CI) plots. (**B**) B16OVA cells pre-treated with 100 nM DAC for five days were trypsinized and plated in 12 well plates with equal numbers of viable cells. Cells were then treated with BLM (0.5 μM) for one day prior to co-cultured with OT-I T cells. The first lane displays the crystal violet staining images (Scale bars, 400 μm). The second lane presents the representative images of cancer cells apoptosis after co-culture with OT-I T cells. (**C**) Quantification of the percentages of early and late apoptotic cells among cancer cells from (**B**), n=3 per group. (**D-F**) Treatment of B16F10 tumors with DNMT1 inhibitor (DAC) or vehicle control in combination with BLM or vehicle control, n=6 per group. Mice weight (**D**), tumor volume (**E**) and tumor weight (**F**), n=6 per group. Data are shown as mean ± SD. **P* < 0.05, ****P* < 0.001, and ns, no significance compared to the

vehicle group by one-way ANOVA (**E** and **F**) and unpaired t test (**C**); #P < 0.05, ##P < 0.01 and ###P < 0.001 between the indicated groups by unpaired t test (**E** and **F**).

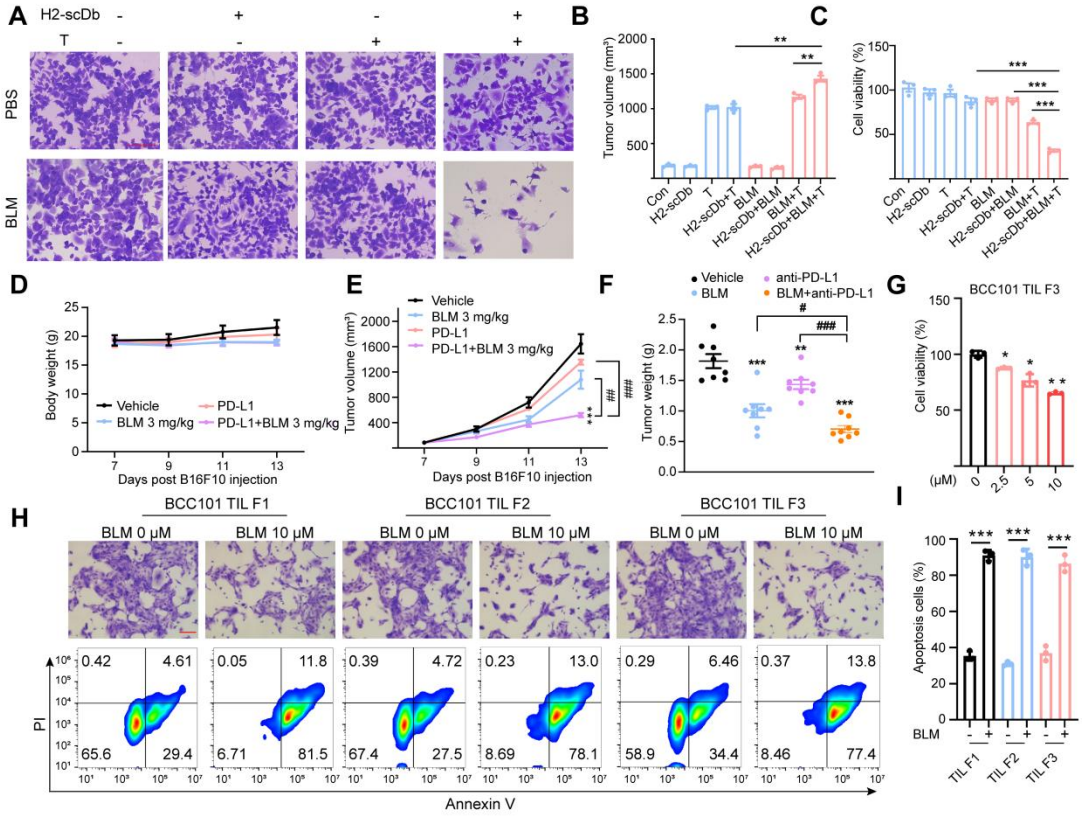

Figure 7. BLM-mediated potentiation of anti-tumor responses for immunotherapy. (**A**) Co-culture of SK-BR-3 cells and human $CD8^+$ T cells for T cell cytotoxicity assay. The crystal violet staining images of remaining cancer cells are displayed (Scale bars, 400 μm). (**B**) The concentration of IFN-γ in the co-culture supernatant as detected by ELISA, n=3 per group. (**C**) T cell activation mediated by BLM and H2-scDb in response to SK-BR-3 cells at E:T ration of 2:1 as measured by the CellTiter-Glo reagent. (**D-F**) Treatment of B16F10 tumors with BLM or vehicle control in combination with PD-L1 or isotype control antibodies, n=8 per group. (**D**) Mice weight, (**E**) tumor volumes and (**F**) tumor weights of mice. (**G**) Co-culture of primary bladder cancer cells and TILs for T cell cytotoxicity assay. Primary bladder cancer cells were pre-treated with indicated concentrations of BLM for 24 h. Percent remaining live

cancer cells following 24 h incubation with autologous TILs at a 1:5 ratio. (**H**) Co-culture of patient-derived tumor cells BCC101 and TILs (F1, F2 and F3 fragments) for T cell cytotoxicity assay. BCC101 tumor cells were pre-treated with BLM (10 μM) for 24 h prior to co-culture with TILs. The first lane displays the crystal violet staining images (Scale bars, 400 μm). The second lane presents the representative images of cancer cells apoptosis after co-culture with TILs. (**I**) Quantification of the percentages of early and late apoptotic cells among cancer cells from (**H**), n=3 per group. Data are shown as mean ± SD. **P* < 0.05, ***P* < 0.01, ****P* < 0.001, and ns, no significance compared to the vehicle group by unpaired t test (**B**, **C**, and **I**) and one-way ANOVA (**E**-**G**); #*P* < 0.05, ##*P* < 0.01 and ###*P* < 0.001 between the indicated groups by unpaired t test (**E** and **F**).